View metadata, citation and similar papers at core.ac.uk

brought to you by CORE

provided by NASA Technical Reports Server

NASA Technical Paper 2987

June 1990

Improved Model for Solar Cosmic Ray Exposure in Manned Earth Orbital Flights

John W. Wilson,
John E. Nealy,
William Atwell,
Francis A. Cucinotta,
Judy L. Shinn,
and Lawrence W. Townsend

(NASA-TP-2987) IMPROVED MODEL FOR SOLAR COSMIC RAY EXPOSURE IN MANNED EARTH ORBITAL FLIGHTS (NASA) 14 p CSCL 03B

N90-25031

Unclas
H1/93 0264751

NASA

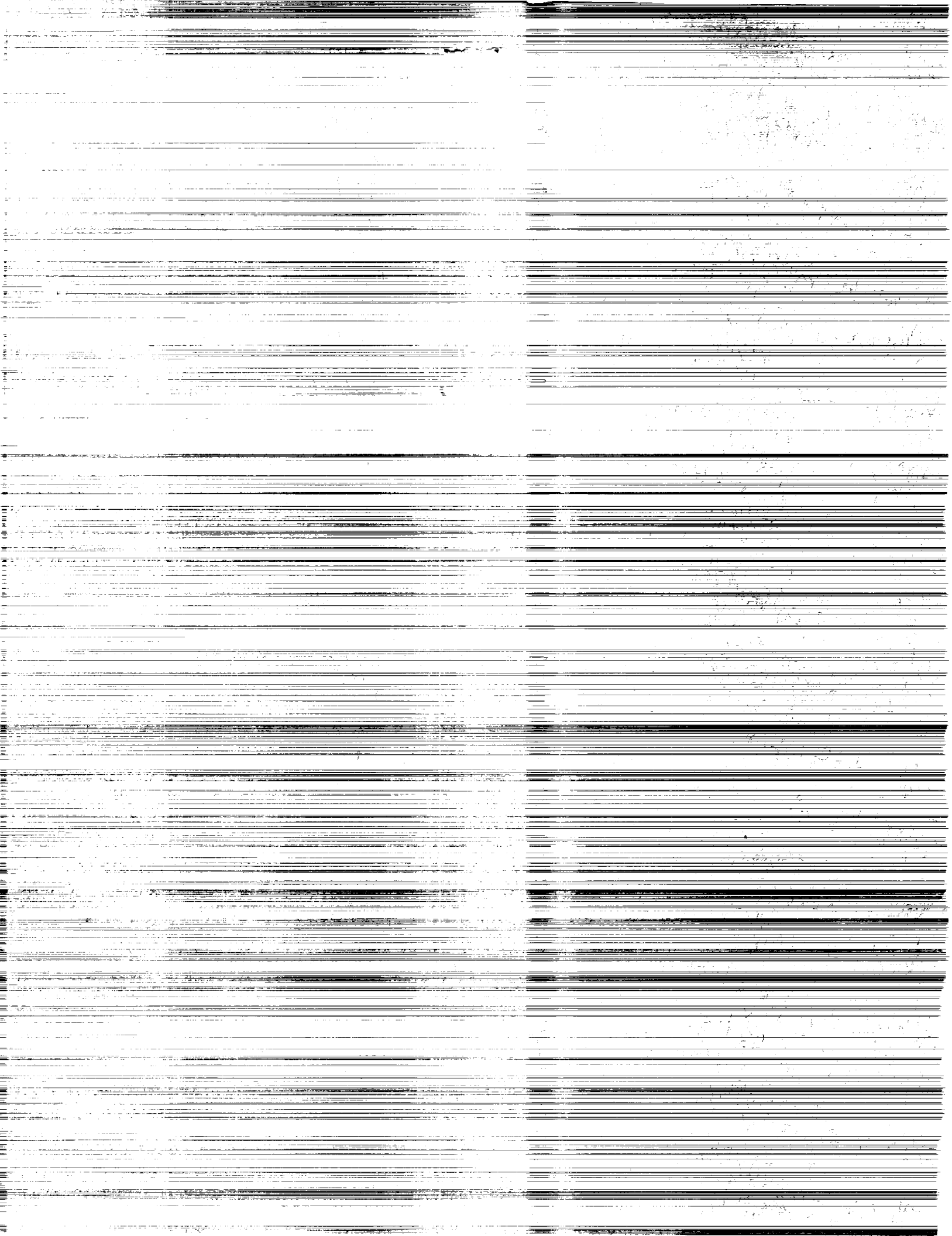

NASA Technical Paper 2987

1990

Improved Model for Solar Cosmic Ray Exposure in Manned Earth Orbital Flights

John W. Wilson
and John E. Nealy
Langley Research Center
Hampton, Virginia

William Atwell
and Francis A. Cucinotta
Rockwell International
Space Transportation Systems Division
Houston, Texas

Judy L. Shinn
and Lawrence W. Townsend
Langley Research Center
Hampton, Virginia

NASA
National Aeronautics and Space Administration
Office of Management
Scientific and Technical Information Division

Abstract

A calculational model is derived for use in estimating Solar cosmic ray exposure to critical body organs in low Earth orbit at the center of a large spherical shield of fixed thickness. The effects of the Earth's geomagnetic field and the astronauts' self-shielding are evaluated explicitly. The geomagnetic field model is an approximate tilted eccentric dipole with geomagnetic storms represented as an impressed uniform field. The storm field is related to the planetary geomagnetic index K_p. The Shuttle geometry is introduced into the resultant computer code using the Shuttle mass distribution surrounding two locations on the flight deck. The Shuttle is treated as pure aluminum and the astronaut as soft tissue. Short-term average fluence over a single orbit is calculated as a function of the location of the lines of nodes or long-term averages over all lines of nodes for a fixed inclination.

Introduction

Solar cosmic rays observed in low Earth orbit first passed through the Earth's magnetic field. Those particles that are able to penetrate the geomagnetic field must further penetrate the walls of the spacecraft before exposing the human occupants. As a result of interactions in the vehicle structure and the bulk tissues of the astronauts' bodies, the composition of the rays is greatly altered. Any reasonable estimate must account for geomagnetic effects, the atomic and nuclear interactions, and the spacecraft and human body geometry.

During times of increased solar activity, small amounts of the solar plasma are ejected into interplanetary space. When this plasma interacts with the Earth's magnetic field, large distortions of this field result in geomagnetic storms. Since the energetic solar flare particles often arrive during such geomagnetic disturbances, the penetration of the energetic protons into the magnetospheric cavity can be vastly different from that seen under quiet conditions.

In a previous report (ref. 1), we derived a simple model for estimating exposure to the critical organs of an astronaut within a large spherical shield using a centered-tilted dipole model of the geomagnetic field and an approximate geomagnetic storm field as an impressed uniform field. In the present work, approximate expressions are derived for a tilted eccentric dipole model. Geomagnetic model parameters are used to better approximate the recently calculated worldwide vertical cutoffs of Shea and Smart (ref. 2) for the 1980 magnetic field parameters than in the previous study (ref. 1). The average transmission factors of the approximate model agree well with the transmission factors of Smart and Shea (ref. 3). The approximate orbit-averaged transmission factors are found as a function of location of the ascending line of nodes, and dose is given for the worst-case exposed orbit for various geomagnetic storm conditions. A comparison is made with earlier work.

A necessary requirement for space mission analysis is a reliable method of calculating the anticipated dose distribution in the human body. In the case of extraterrestrial radiations, a model is required for evaluating the effects of the geomagnetic field in addition to the interaction with the spacecraft structure and the human body. Described herein are additional computer subroutines which calculate the proton dose within the Shuttle averaged over five major segments (upper limbs, lower limbs, upper trunk, lower trunk, and skull) of the blood-forming organs (BFO), ocular lens, and skin by treating the human body and vehicle geometry in detail (refs. 4 and 5) but assuming isotropicity of the incident primary particles. The calculation uses an approximate form of transport theory in which nuclear star effects are incorporated (refs. 1 and 6). The output of the program is in terms of physical dose and dose equivalent.

Geomagnetic Effects on Orbital Environment

Charged particles arriving at some location within the geomagnetosphere are deflected by the Lorentz force $e\mathbf{v} \times \mathbf{B}$ which prevents penetration for some directions of incidence and some energies. Such phenomena were extensively studied by Störmer (ref. 7) for a dipole magnetic field which provides the basis for classifying the orbital trajectories of charged particles arriving at some location within the field. As a part of Störmer's theory, there exist allowed trajectories with no connection to asymptotic trajectories now recognized as trapping regions

associated with Van Allen radiation. Numerical solutions to the charged particle equations of motion in more realistic geomagnetic field models were introduced by McCracken (ref. 8) and further advanced by Smart and Shea (refs. 2, 3, and 9). Our purpose here will not be to supplant the vastly detailed numerical work but to seek a simple analytic form to reasonably approximate the more general numerical solutions.

The geomagnetic field can be reasonably approximated by a tilted dipole with moment $M = r_e^3 31\,500$ nT displaced from the Earth's center by 430 km or $0.068 r_e$ where $r_e = 6378$ km. The tilt angle is 11.7° at 69° W longitude. The magnetic quadrupole contributions are then about 10 percent at the surface and decrease to 5 percent at $2r_e$. Higher-order moments are even smaller. The motion of charged particles in the geomagnetic field was studied extensively by Störmer. We outline his methods herein. In spherical coordinates, Störmer showed that the azimuth ϕ is an ignorable coordinate possessing an integral for the particles trajectory such that

$$\cos\omega = \frac{\gamma}{mvr\sin\theta} - \left(\frac{ZeM}{mvc}\right)\frac{\sin\theta}{r^2} \tag{1}$$

where m is the mass of the particle, Ze is the charge, v is the velocity, c is the velocity of light, r is radial distance from the center of the field, θ is colatitude, γ is an integration constant, and ω is the angle between the velocity vector and the azimuthal direction. The allowed Störmer regions consist of the space for which

$$|\cos\omega| \equiv \left|\frac{\gamma}{mvr\ \sin\ \theta} - \left(\frac{ZeM}{mvc}\right)\frac{\sin\theta}{r^2}\right| \leq 1 \tag{2}$$

Further analysis of the condition in equation (2) shows stable trapping regions as well as the Störmer main cone of transmission given for $\gamma = 2mv(ZeM/mvc)^{1/2}$. The Störmer main cone is given (ref. 10) by the solid angle element

$$\Omega = 2\pi(1 + \cos\omega) \tag{3}$$

which contains the allowed directions of arrival for particles of rigidity R (momentum per unit charge) given by

$$R = \frac{M}{c}\frac{\sin^4\theta}{r^2\left[1 + (1 - \sin^3\theta\cos\omega)^{1/2}\right]^2} \tag{4}$$

Henceforth we replace the colatitude θ by the magnetic latitude λ_m and note that Ω varies from 0 to 4π reaching its half-value at $\omega = \pi/2$ including angles up to the vertical direction. The vertical cutoff model is expressed as

$$\Omega \approx 4\pi\, U\left[R - R_C\left(\lambda_m\right)\right] \tag{5}$$

where the vertical cutoff rigidity from equation (4) is

$$R_C\left(\lambda_m\right) = \frac{M}{4cr^2}\cos^4\lambda_m \tag{6}$$

and $U(x)$ is the unit step function.

Not included in the above formalism are those trajectories which are cut off by the shadow cast by the solid Earth. The fraction of the solid angle covered by the Earth's shadow is estimated, assuming that the curvature of the local trajectories is large compared with the Earth's radius (ref. 10). Then the solid angle fraction is

$$\frac{\Omega_{\text{sh}}}{4\pi} = \frac{1}{2}\left[1 + \cos\left(\sin^{-1}\frac{1}{r}\right)\right] \tag{7}$$

The corrected solid angle for the vertical cutoff model is then

$$\Omega = \Omega_{\text{sh}} U\left[R - R_C\left(\lambda_m\right)\right] \tag{8}$$

which leaves the local solid angle open to transmission of charged particles of rigidity R at altitude r and geomagnetic latitude λ_m.

Spacecraft in low Earth orbit (LEO) are typically in circular orbits which simplifies the analysis. The orbit plane is inclined with respect to the equatorial plane. Since the Earth's angular momentum (spin) and the spacecraft orbital angular momentum are conserved, the angle between them is fixed and equal to the inclination angle i. The magnetic axis rotates with the Earth and therefore precesses about the rotational axis within a 24-hour period. The geographic location of the ascending node likewise moves around the geographic equator every 24 hours. The inclination of the orbit plane relative to the magnetic axis i_m likewise is periodic. If η is the geographic coordinate of the ascending node line, then

$$\cos i_m = \cos i\cos\theta_m + \sin i\sin\theta_m\cos\left(\eta - \phi_m - 90°\right) \tag{9}$$

where θ_m and ϕ_m are the magnetic north pole colatitude and longitude. The average transmission factor around this orbit $\overline{F}$ is then

$$\overline{F}(R, i, \eta) = \frac{\Omega_{\text{sh}}}{i_m}\int_o^{i_m} U\left[R - R_C(\lambda)\right] d\lambda = \frac{i_m - \lambda_m}{i_m}\Omega_{\text{sh}} \tag{10}$$

where λ_m is the magnetic latitude with cutoff at R as given by

$$R_C(\lambda_m) = R \tag{11}$$

We note that i_m goes through a maximum and minimum orbit corresponding to $\eta_{\max} = \phi_m - 90°$ and $\eta_{\min} = \phi_m + 90°$ for which $i_m = i + \theta_m$ and $i_m = |i - \theta_m|$, respectively, as we have shown elsewhere (ref. 1).

We may also calculate the long-term average over many days of orbits by averaging equation (10) over the node angle η as

$$\overline{F}(R,i) = \frac{1}{\pi}\int_0^{\pi} \Omega_{\text{sh}} \frac{i_m - \lambda_m}{i_m}\, d_\eta = \frac{1}{\pi}\int_{\phi_\lambda}^{\pi} \Omega_{\text{sh}} \frac{i_m - \lambda_m}{i_m}\, d\phi \quad (12)$$

where

$$\cos i_m = \cos i \cos\theta_m + \sin i \sin\theta_m \cos\phi \quad (13)$$

and

$$\phi_\lambda = \begin{cases} 0 & (\lambda_m \le |i - \theta_m|) \\ \cos^{-1}\left[\dfrac{\cos\lambda_m - \cos i\cos\theta_m}{\sin i \sin\theta_m}\right] & (|i-\theta_m| \le \lambda_m \le i + \theta_m) \\ \pi & (\lambda_m > i + \theta_m) \end{cases} \quad (14)$$

Equation (12) may be rewritten as

$$\overline{F}(R,i) = \Omega_{\text{sh}}\left[\left(1 - \frac{\phi_\lambda}{\pi}\right) - \frac{1}{\pi}\int_{\phi_\lambda}^{\pi} \frac{\lambda_m}{i_m}\, d\phi\right] \quad (15)$$

where the last integral is approximated by a numerical quadrature. The results of equation (15) are compared with the numerical calculations of Smart and Shea for 400-km (216-n.mi.) orbits at several inclinations in figure 1 for this centered dipole field model with $\theta_m = 11.7°$ (tilt angle) and longitude $\phi_m = -69°$ (69°W).

An important correction to the centered dipole field is the displacement of the geomagnetic dipole 430 km (232 n.mi.) from the Earth's center. Unfortunately, the formalism is very complicated, since the distance r from the dipole center is no longer constant even for a circular orbit. The offset dipole decreases the cutoffs in the Atlantic hemisphere defined by the meridinal plane normal to the tilt direction and increases the cutoffs in the remaining hemisphere over the Pacific. We define two cutoff functions for centered dipole fields as

$$R_j(\lambda_m) = \frac{14.9}{(r + \delta_j)^2}\cos^4\lambda_m \quad (16)$$

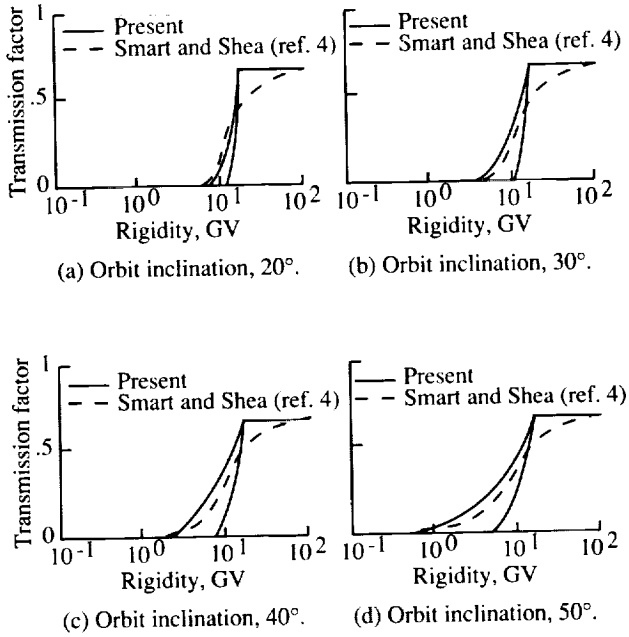

(a) Orbit inclination, 20°. (b) Orbit inclination, 30°.

(c) Orbit inclination, 40°. (d) Orbit inclination, 50°.

Figure 1. Dipole maximum and minimum cutoff model and numerical simulation of exact geomagnetic field model.

where $j = A$, $\delta_A = 593$ km (320 n.mi.) for the Atlantic hemisphere; $j = P$, $\delta_P = -504$ km (-272 n.mi.) for the Pacific; λ_m is the usual magnetic latitude which depends on the hemisphere; and r is the geocentric radius of the orbit. The value 14.9 GV is found from the value of the dipole moment of r_e^3 31 500 nT, and δ_j were chosen to match the minimum equatorial cutoff in the Atlantic region of Shea and Smart (ref. 9) and the maximum cutoff in the Pacific. The calculation of the orbit average transmission factor is as before except that the two hemispheres are considered separately as

$$\overline{F}(R,i,\eta) = \frac{1}{2}\Omega_{\text{sh}}\left[\frac{i_m - \lambda_A}{i_m} + \frac{i_m - \lambda_P}{i_m}\right] \quad (17)$$

where

$$R_A(\lambda_A) = R \quad (18)$$

and

$$R_P(\lambda_P) = R \quad (19)$$

Similarly, the long-term average of equation (12) is extended to each hemisphere as

$$\overline{F}(R,i) = \frac{\Omega_{\text{sh}}}{2\pi}\left[\int_{\phi_A}^{\pi}\left(\frac{i_m - \lambda_A}{i_m}\right) d\phi + \int_{\phi_P}^{\pi}\left(\frac{i_m - \lambda_P}{i_m}\right) d\phi\right] \quad (20)$$

where the integrals are evaluated as described for equation (15). The average transmission factors of equation (20) are compared with the numerical calculations of Smart and Shea (ref. 3) in figure 2. The pole's tilt angles (ref. 11) are given in table 1

along with suitably chosen longitudes and are shown in relation to the vertical cutoff rigidities of Smart and Shea in figures 3 and 4.

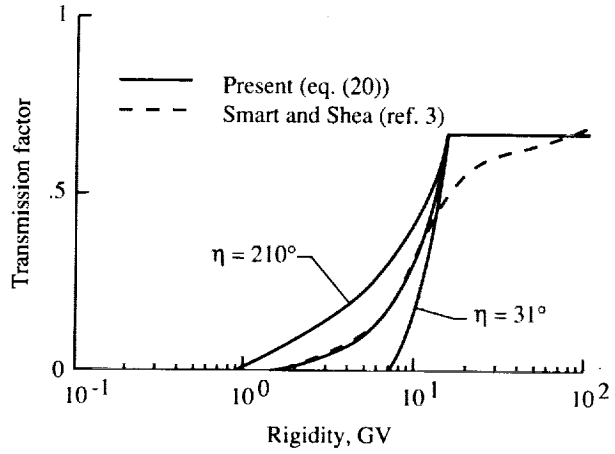

(a) Orbit inclination, 40°.

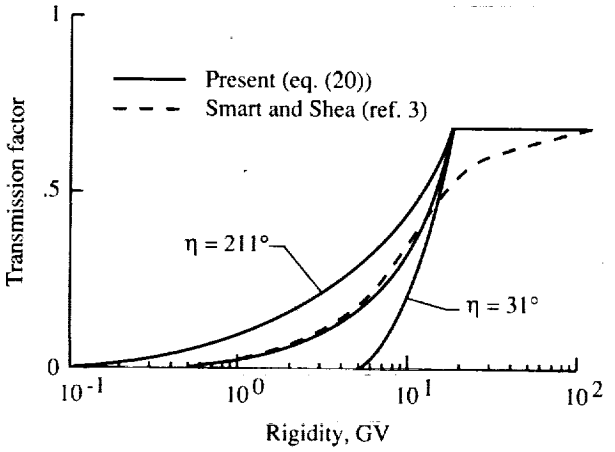

(b) Orbit inclination, 50°.

Figure 2. Offset dipole model average transmission factors with detailed calculations of Smart and Shea (ref. 3) and maximum and minimum transmission factors.

Table 1. Geographic Locations of Offset Poles in Present Calculations

Magnetic pole	Longitude, ϕ_m, deg	Tilt, θ_m, deg
North	−69	16
South	121	22

During times of intense solar activity, the solar plasma emitted in solar flares and subflares advances outward and arrives at 1 AU from the Sun. If the Earth is locally present, the plasma interacts with the geomagnetic field in which the plasma pressure performs work on the local geomagnetic field. The initial impact produces hydromagnetic waves causing a general increase in geomagnetic intensity. As plasma flow is established, it generates large electric ring currents and a corresponding impressed magnetic storm field. In the initial phase (hydromagnetic wave), the storm field is parallel to the equatorial field after which the storm field reverses in the main phase of the storm caused by ring currents within the magnetopause and opposes the quiet field, to cause a net decrease of the field strength. The main phase is followed by slow recovery to the quiet field conditions (ref. 11).

The magnetic storm model used here assumes a uniform magnetic field impressed on the normal quiet field (ref. 10). The storm field strength can be found from the change in the horizontal field component around the geomagnetic equator. We represent this field by H_{st}. Typical values of H_{st} in the main phase range from substorm values −10 nT to severe storms with −500 nT. On rare occasions, for very intense storms, the storm field exceeds −1000 nT.

Magnetic disturbances have been observed for many years, and various classification schemes for such disturbances have been proposed. The planetary magnetic index K_p is based on magnetometer measurements of 12 stations worldwide. The K_p index is related to a derived planetary index a_p and storm field strength by Bartels (ref. 11) given in table 2.

Table 2. Relation of Magnetic Indices to Magnetic Storm-Field Strength

K_p	a_p	$\lvert H_{st}\rvert$,nT
0	0	0
1	4	8
2	7	14
3	15	30
4	27	54
5	48	96
6	80	160
7	132	264
8	207	414
9	400	800

The vertical cutoff rigidity as given by equation (16) is further modified to approximate the effects of geomagnetic disturbances. It was shown by

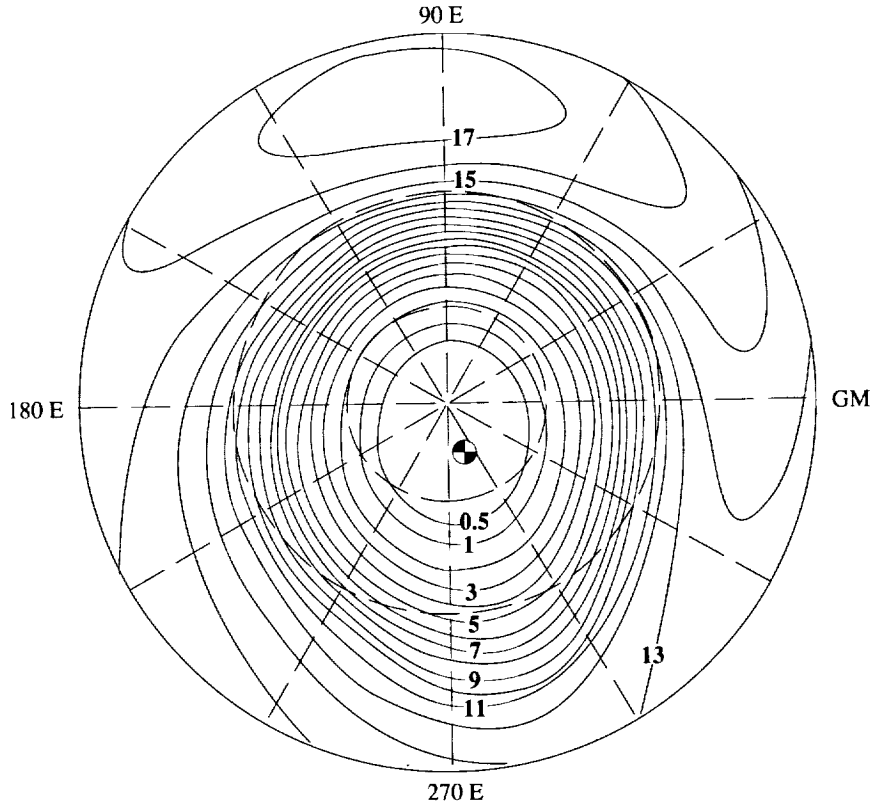

Figure 3. Vertical cutoff contours in northern hemisphere showing location of North magnetic pole.

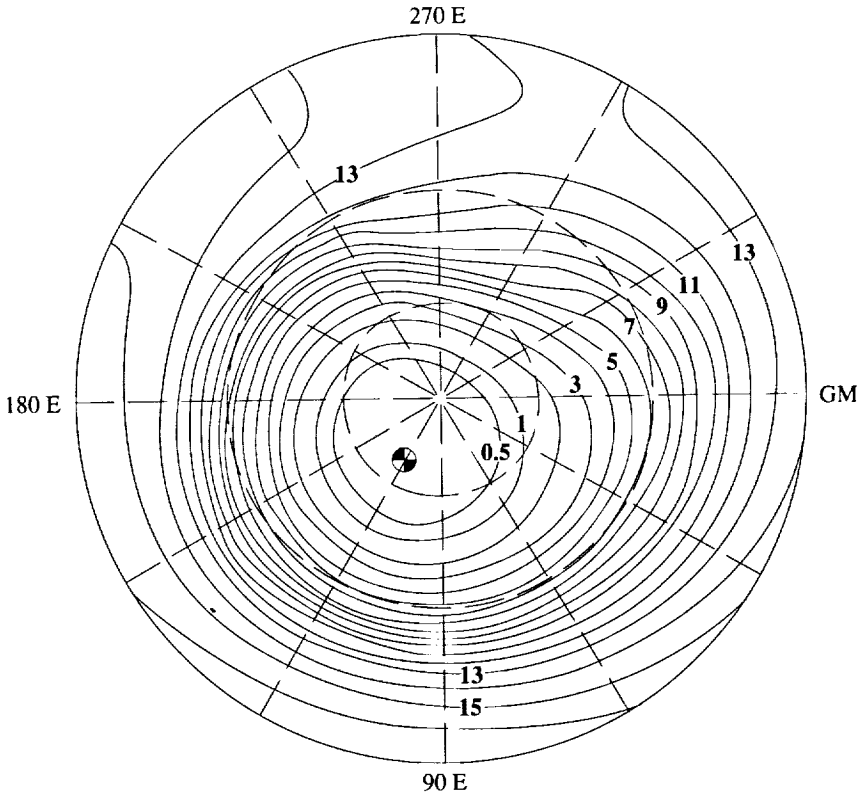

Figure 4. Vertical cutoff contours in southern hemisphere showing location of South magnetic pole.

Kuhn, Schwamb, and Payne (ref. 10) that the appropriate equation is

$$R_C(\lambda_m) = \frac{14.9}{r^2}\cos^4\lambda_m\left[1 + \frac{H_{st}r^3}{M}\left(\frac{4}{\cos^6\lambda_m} - 1\right)\right] \quad (21)$$

for the centered dipole field. In the context of our approximation of the offset-tilted dipole field, we get

$$R_j(\lambda_m) = \frac{14.9}{\left(r+\delta_j\right)^2}\cos^4\lambda_m\left[1 + \frac{H_{st}\left(r+\delta_j\right)^3}{M}\left(\frac{4}{\cos^6\lambda_m} - 1\right)\right] \quad (22)$$

This vertical cutoff replaces equation (16) and applies to storm conditions. Note that the cutoff is zero whenever the result of equation (22) is negative. The corresponding transmission factor on the worst case orbit ($\eta \approx 211°$) is shown in relation to the quiet field average transmission factors of Smart and Shea (ref. 3) in figure 5.

Dose Estimation

In passing through tissue, energetic protons interact mostly through ionization of atomic constituents by the transfer of small amounts of momentum to orbital electrons. Although the nuclear reactions are far less numerous, their effects are magnified because of the large momentum transferred to the nuclear particles and the struck nucleus itself. Unlike the secondary electrons formed through atomic ionization by interaction with the primary protons, the radiations resulting from nuclear reactions are mostly heavy ionizing and generally have large biological effectiveness. Many of the secondary particles of nuclear reactions are sufficiently energetic to promote similar nuclear reactions and thus cause a buildup of secondary radiations. The description of such processes requires solution of the transport equation. The approximate solutions for the transition of protons in 30-cm-thick slabs of soft tissue for fixed incident energies have been made (ref. 6). The results of such calculations are dose conversion factors for relating the primary monoenergetic proton fluence to dose or dose equivalent as a function of position in a tissue slab.

Whenever the radiation is spatially uniform, the dose at any point x in a convex object may be calculated (ref. 12) by

$$D(x) = \int_0^\infty \int_\Omega R_n\left[z_x(\Omega), E\right]\phi(\Omega, E)\, d\Omega\, dE \quad (23)$$

where $R_n(z, E)$ is the dose at depth z for normal incident protons of energy E on a tissue slab, $\phi(\Omega, E)$ is the local differential proton fluence along direction Ω, and $z_x(\Omega)$ is the distance from the boundary

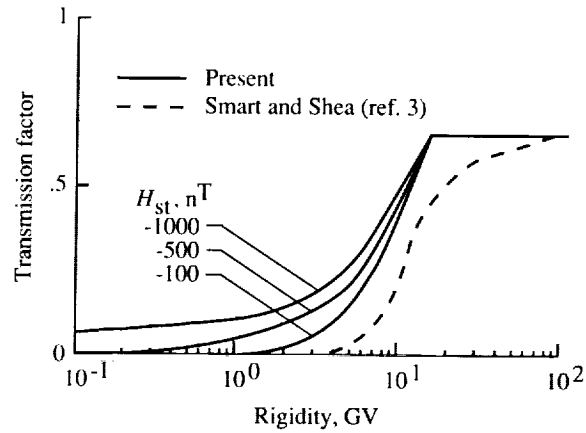

(a) Orbit inclination, 30°.

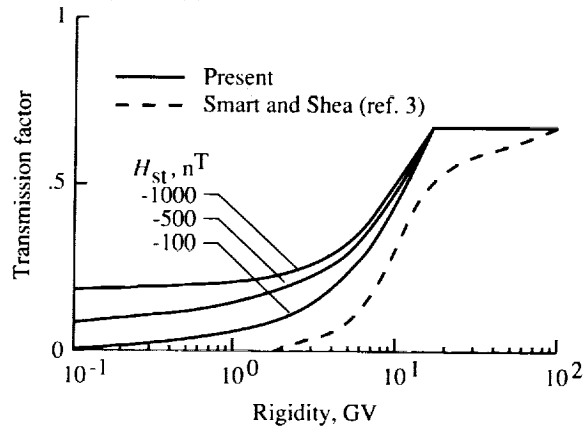

(b) Orbit inclination, 40°.

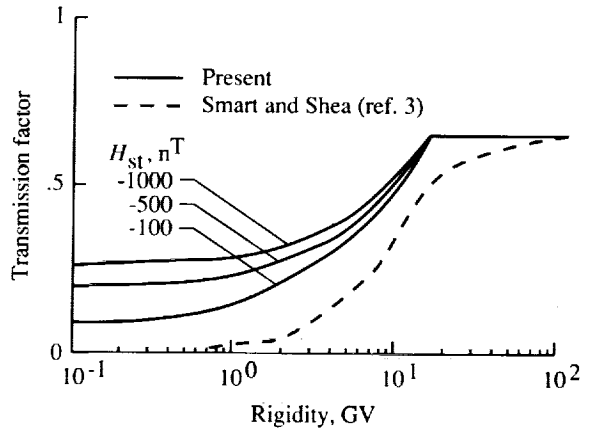

(c) Orbit inclination, 50°.

Figure 5. Maximum transmission factor for various storm fields and quiet time average transmission of Smart and Shea. $\eta = 211°$.

along Ω to point x. It has been shown that equation (23) always overestimates the dose but is an accurate estimate when the ratio of the proton beam divergence due to nuclear reaction to the bodies' radius of curvature is small (ref. 12). Equation (23) is a practical prescription for introducing nuclear reaction effects into calculations of dose in geometrically complex objects such as the human body. The main requirement is that the dose conversion factors for a tissue slab be adequately known for a broad range of energies and depths. The dose conversion factors for tissue were derived in reference 6, and a correction for an aluminum shield was found in reference 1. The spacecraft geometry is taken as an aluminum sphere of large radius.

Method for Shuttle Geometry

In the previous section, the calculation of astronaut exposure in the center of a large aluminum sphere of arbitrary thickness was derived for a specific orbit with either the quiet geomagnetic field or with a geomagnetic disturbance. We denote that result by $D_{\mathrm{sph}}(t_s)$, and it has a different value for each critical organ for which exposure within the aluminum sphere of thickness t_s is evaluated. Within the context of assumed isotropic radiation, the exposure at some location within the Shuttle is

$$D = \int_0^\infty D_{\mathrm{sph}}(t_s)\, f(t_s)\, dt_s \qquad (24)$$

where $f(t_s)$ describes the mass distribution of the Shuttle structure assumed to be aluminum about that particular location. Physically, $f(t_s)\, dt_s$ is the solid angle fraction for which the areal density to the Shuttle surface lies between t_s and $t_s + dt_s$. The cumulative distribution of areal density is given by

$$F_C(t_s) = \int_0^{t_s} f(t_s)\, dt_s \qquad (25)$$

and is shown for two locations in the Shuttle (ref. 5) in figure 6. Also shown in figure 6 are the following approximate functions:

$$f_1(t_s) = \begin{cases} \dfrac{0.176}{t_s} & (1 \le t_s \le 2) \\ \dfrac{0.113}{t_s} & (2 \le t_s \le 20) \\ \dfrac{0.353}{t_s} & (20 \le t_s \le 120) \end{cases} \qquad (26)$$

and

$$f_2(t_s) = \begin{cases} \dfrac{0.303}{t_s} & (1 \le t_s \le 6) \\ \dfrac{0.147}{t_s} & (6 \le t_s \le 132) \end{cases} \qquad (27)$$

where the functions are understood to be zero outside of specified ranges. Formulas (24), (26), and (27) are used in conjunction with the methods described in previous sections to estimate Shuttle exposure in the two locations referred to in reference 5 as dosimeter location numbers 1 and 2 which comprise the most and the least shielded locations in the Shuttle crew compartment, respectively. The method can be easily expanded to include more astronaut organs and other Shuttle locations.

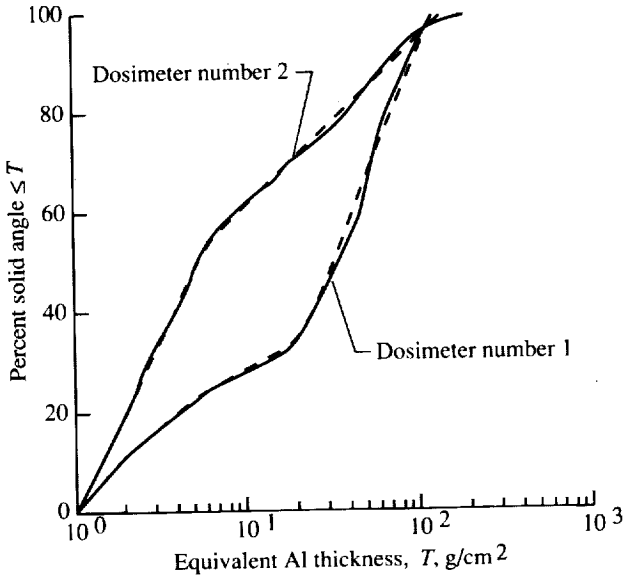

Figure 6. Mass distribution of two locations on Shuttle flight deck.

Results

The maximum exposure limits in force for the Space Station *Freedom* (ref. 13) are shown in table 3. The dose and dose equivalent to critical body organs for an aluminum shield 1 g/cm^2 thick are shown in tables 4 through 7 for various storm conditions (H_{st}). The exposures are shown for a worst-exposed orbit ($\eta = 211°$) and the average over all η. The average is shown, since average transmission factors are calculated by several groups, and one may be tempted to use the transmission factor appropriate for the galactic cosmic ray background (refs. 14 and 15). It is clear from the results in tables 4 through 7 that such use of average cutoffs provides exposure estimates which could be too small by a

factor of 2 to 10. Such an underestimate is clearly unacceptable. Furthermore, comparing the current dose estimates with values for transmission factors derived for a tilted concentric dipole field (ref. 1), we see that the dose values of the current field model are a factor of 3 to 5 higher. The eccentric field had two effects which lower the cutoffs. The offset displaces the South magnetic pole to lower latitudes and lowers the geomagnetic cutoff values over the Atlantic. The methods derived herein allow evaluating exposures as a function of the location of the line of nodes and should provide acceptable estimates of exposure.

Table 3. Ionizing Radiation Exposure Limits for Space Station *Freedom* Astronauts

Exposure interval	Dose equivalent, cSv, for—		
	Skin	Eye	Blood-forming organs
30 days	150	100	25
Annual	300	200	50
Career	600	400	[a]100–400

[a]Dependent on gender and age at initial exposure.

Observing the levels of exposure in low inclination orbits ($i \approx 30°$), a significant exposure could clearly occur if particle arrivals coincided with a large magnitude ($K_p \approx 9$) magnetic disturbance. On the basis of the present analysis, a more in-depth study of potential solar flare exposure of the Space Station *Freedom* seems warranted. Such a study should include a review of the history of major geomagnetic disturbances in proximity to solar particle events, a review of alternate geomagnetic storm models, and a review of the specific Space Station *Freedom* shield geometry.

The exposure for Shuttle flight in a 400-km (216-n.mi.) orbit with a 50° inclination are shown in table 8 for the February 23, 1956, solar event spectrum as compiled by Foelsche et al. (ref. 16). A magnetic storm was assumed to be in progress with an impressed field of −100 nT. The results shown in table 8 are for the long-term, average geomagnetic cutoffs, since these are directly comparable with the work of other geomagnetic models (refs. 14 and 15). We note, however, that actual exposure could be greatly different depending on the location of the line of nodes at the time of arrival of the high-energy flare particles.

Concluding Remarks

The present code should be useful for assessing the potential exposure in low Earth orbit missions if the Solar spectrum and state of the geomagnetic field are known.

It was shown for low inclination orbits ($i \approx 30°$) that a significant exposure could occur if the particle's arrival coincided with a large magnitude ($K_p \approx 9$) magnetic disturbance. On the basis of the present analysis, a more in-depth study of potential solar flare exposure of Space Station *Freedom* seems warranted. Such a study should include a review of the history of major geomagnetic disturbances in proximity to solar particle events, a review of alternate geomagnetic storm models, and specific Space Station *Freedom* shield geometry.

NASA Langley Research Center
Hampton, VA 23665-5225
April 17, 1990

Table 4. Skin Dose Behind Aluminum Shield 1 g/cm^2 Thick During February 25, 1956, November 12–13, 1960, and August 4, 1972, Events With Various Storm Fields

Inclination, deg	Skin dose, cGy, during—								
	Feb. 1956 for H_{st}, nT, of—			Nov. 1960 for H_{st}, nT, of—			Aug. 1972 for H_{st}, nT, of—		
	−100	−500	−900	−100	−500	−900	−100	−500	−900
30, max	< 0.1	2.2	12.0	0	4.9	34.0	0	15.0	100.0
30, avg	< .1	.3	2.6	0	.5	7.1	0	1.6	22.0
40, max	2.9	19.0	28.0	6.3	53.0	79.0	19.0	170.0	240.0
40, avg	.4	5.4	9.8	.8	15.0	28.0	2.3	47.0	86.0
50, max	17.0	31.0	39.0	47.0	89.0	111.0	140.0	280.0	340.0
50, avg	4.8	13.0	18.0	13.0	36.0	51.0	39.0	110.0	160.0

Table 5. Skin Dose Equivalent Behind Aluminum Shield 1 g/cm^2 Thick During February 25, 1956, November 12–13, 1960, and August 4, 1972, Events With Various Storm Fields

Orbit inclination, deg	Skin dose equivalent, cSv, during—								
	Feb. 1956 for H_{st}, nT, of—			Nov. 1960 for H_{st}, nT, of—			Aug. 1972 for H_{st}, nT, of—		
	−100	−500	−900	−100	−500	−900	−100	−500	−900
30, max	< 0.1	3.3	17.0	0	7.0	49.0	0	20.0	140.0
30, avg	< .1	.4	3.7	0	.7	10.0	0	2.1	30.0
40, max	4.3	27.0	39.0	8.9	78.0	110.0	25.0	230.0	333.0
40, avg	.7	7.7	14.0	1.1	22.0	40.0	3.1	63.0	120.0
50, max	24.0	44.0	54.0	68.0	130.0	160.0	200.0	380.0	470.0
50, avg	6.8	18.0	25.0	18.0	52.0	74.0	53.0	150.0	220.0

Table 6. BFO Dose Behind Aluminum Shield 1 g/cm^2 Thick During February 25, 1956, November 12–13, 1960, and August 4, 1972, Events With Various Storm Fields

Orbit inclination, deg	BFO dose, cGy, during –								
	Feb. 1956 for H_{st}, nT, of–			Nov. 1960 for H_{st}, nT, of			Aug. 1972 for H_{st}, nT, of–		
	−100	−500	−900	−100	−500	−900	−100	−500	−900
30, max	< 0.1	1.0	3.3	0	.9	4.4	0	1.8	10.0
30, avg	< .1	.2	.8	0	.1	1.0	0	.2	2.3
40, max	1.4	4.9	6.8	1.3	6.7	9.5	2.5	16.0	24.0
40, avg	.3	1.5	2.5	.2	2.0	3.4	.4	4.7	8.8
50, max	4.6	7.6	9.3	6.2	11.0	13.0	15.0	27.0	33.0
50, avg	1.5	3.2	4.4	1.8	4.4	6.2	4.2	11.0	16.0

Table 7. BFO Dose Equivalent Behind Aluminum Shield 1 g/cm^2 Thick During February 25, 1956, November 12–13, 1960, and August 4, 1972, Events With Various Storm Fields

Orbit inclination, deg	BFO dose equivalent, cSv, during –								
	Feb. 1956 for H_{st}, nT, of–			Nov. 1960 for H_{st}, nT, of–			Aug. 1972 for H_{st}, nT, of–		
	−100	−500	−900	−100	−500	−900	−100	−500	−900
30, max	< 0.1	1.7	5.1	0	1.3	6.1	0	2.6	15.0
30, avg	< .1	.3	1.2	0	.2	1.3	0	.3	3.3
40, max	2.3	7.6	10.0	1.8	9.2	13.0	3.6	23.0	34.0
40, avg	.5	2.3	3.9	.3	2.7	4.7	.5	6.7	12.0
50, max	7.3	12.0	14.0	8.5	15.0	18.0	21.0	38.0	48.0
50, avg	2.3	5.0	6.9	2.5	6.1	8.6	6.0	15.0	22.0

Table 8. Human Exposure at Two Locations in Shuttle Crew Compartment for February 23, 1956, Event With H_{st} = −100 nT at 400 km and Orbit Inclination of 50°

Location	Exposure in–					
	BFO		Skin		Lens	
	cGy	cSv	cGy	cSv	cGy	cSv
1	2.6	4.9	4.0	6.8	4.1	7.6
2	3.4	5.9	6.0	9.4	6.0	10.0

References

1. Wilson, John W.; Khandelwal, Govind S.; Shinn, Judy L.; Nealy, John E.; Townsend, Lawrence W.; and Cucinotta, Francis A.: *Simplified Model for Solar Cosmic Ray Exposure in Manned Earth Orbital Flights.* NASA TM-4182, 1990.
2. Shea, M. A.; and Smart, D. F.: A World Grid of Calculated Cosmic Ray Vertical Cutoff Rigidities for 1980.0. *18th International Cosmic Ray Conference—Conference Papers,* MG Sessions, Volume 3, Tata Inst. of Fundamental Research (Colaba, Bombay), 1983, pp. 415–418.
3. Smart, D. F.; and Shea, M. A.: Geomagnetic Transmission Functions for a 400 km Altitude Satellite. *18th International Cosmic Ray Conference—Conference Papers,* MG Sessions, Volume 3, Tata Inst. of Fundamental Research (Colaba, Bombay), 1983, pp. 419–422.
4. Billings, M. P.; and Yucker, W. R.: *The Computerized Anatomical Man (CAM) Model.* NASA CR-134043, 1973.
5. Atwell, William; Beever, E. Ralph; Hardy, Alva C.; and Cash, Bernard L.: A Radiation Shielding Model of the Space Shuttle for Space Radiation Dose Exposure Estimations. *Advances in Nuclear Engineering Computation and Radiation Shielding,* Volume 1, Michael L. Hall, ed., American Nuclear Soc., Inc., c.1989, pp. 11:1–11:12.
6. Wilson, John W.; and Khandelwal, Govind S.: Proton-Tissue Dose Buildup Factors. *Health Phys.,* vol. 31, no. 2, 1976, pp. 115–118.
7. Störmer, Carl: Periodische Elektronenbahnen im Felde eines Elementarmagneten und ihre Anwendung auf Brüches Modellversuche und auf Eschenhagens Elementarwellen des Erdmagnetismus. *Z. Astrophys.,* Bd. 1, 1930, pp. 237–274.
8. McCracken, K. G.: The Cosmic-Ray Flare Effect, *J. Geophys. Res.,* vol. 67, no. 2, Feb. 1962.
   1. Some New Methods of Analysis, pp. 423–434.
   2. The Flare Effects of May 4, November 12, and November 15, 1960, pp. 435–446.
   3. Deductions Regarding the Interplanetary Magnetic Field, pp. 447–458.
9. Shea, M. A.; Smart, D. F.; and Gentile, L. C.: The Cosmic Ray Equator Determined Using the International Geomagnetic Reference Field for 1980.0. *18th International Cosmic Ray Conference Conference Papers,* MG Sessions, Volume 3, Tata Inst. of Fundamental Research (Colaba, Bombay), 1983, pp. 423–426.
10. Kuhn, E.; Schwamb, F. E.; and Payne, W. T.: Solar Flare Hazard to Earth-Orbiting Vehicles. *Second Symposium on Protection Against Radiations in Space,* NASA SP-71, 1965, pp. 429–434.
11. Johnson, Francis S., ed.: *Satellite Environment Handbook,* Second ed. Stanford Univ. Press, 1965.
12. Wilson, John W.; and Khandelwal, G. S.: Proton Dose Approximation in Arbitrary Convex Geometry. *Nucl. Technol.,* vol. 23, no. 3, Sept. 1974, pp. 298–305.
13. *Space Station Program Definition and Requirements, Section 3: Space Station Systems Requirements.* SSP 30000, Section 3, Revision F, Space Station Program Off., May 6, 1988.
14. Curtis, S. B.; Doherty, W. R.; and Wilkinson, M. C.: *Study of Radiation Hazards to Man on Extended Near Earth Missions.* NASA CR-1469, 1969.
15. Adams, James H., Jr.: *Cosmic Ray Effects on Microelectronics,* Part IV. NRL Memo. Rep. 5901 (Revised), Naval Research Lab., Dec. 31, 1987.
16. Foelsche, Trutz; Mendell, Rosalind B.; Wilson, John W.; and Adams, Richard R.: *Measured and Calculated Neutron Spectra and Dose Equivalent Rates at High Altitudes; Relevance to SST Operations and Space Research.* NASA TN D-7715, 1974.

NASA
National Aeronautics and Space Administration

Report Documentation Page

1. Report No.	2. Government Accession No.	3. Recipient's Catalog No.
NASA TP-2987		

4. Title and Subtitle	5. Report Date
Improved Model for Solar Cosmic Ray Exposure in Manned Earth Orbital Flights	June 1990
	6. Performing Organization Code

7. Author(s)	8. Performing Organization Report No.
John W. Wilson, John E. Nealy, William Atwell, Francis A. Cucinotta, Judy L. Shinn, and Lawrence W. Townsend	L-16759
	10. Work Unit No. 199-22-76-01

9. Performing Organization Name and Address	11. Contract or Grant No.
NASA Langley Research Center Hampton, VA 23665-5225	

12. Sponsoring Agency Name and Address	13. Type of Report and Period Covered
National Aeronautics and Space Administration Washington, DC 20546-0001	Technical Paper
	14. Sponsoring Agency Code

15. Supplementary Notes

John W. Wilson, John E. Nealy, Judy L. Shinn, and Lawrence W. Townsend: Langley Research Center, Hampton, Virginia.
William Atwell and Francis A. Cucinotta: Rockwell International, Space Transportation Systems Division, Houston, Texas.

16. Abstract

A calculational model is derived for use in estimating Solar cosmic ray exposure to critical body organs in low Earth orbit at the center of a large spherical shield of fixed thickness. The effects of the Earth's geomagnetic field and the astronauts' self-shielding are evaluated explicitly. The geomagnetic field model is an approximate tilted eccentric dipole with geomagnetic storms represented as an impressed uniform field. The storm field is related to the planetary geomagnetic index K_p. The code is applied to the Shuttle geometry using the Shuttle mass distribution surrounding two locations on the flight deck. The Shuttle is treated as pure aluminum and the astronaut as soft tissue. Short-term average fluence over a single orbit is calculated as a function of the location of the lines of nodes or long-term averages over all lines of nodes for a fixed inclination.

17. Key Words (Suggested by Authors(s))	18. Distribution Statement
Solar flares Geomagnetism Dose equivalent Nuclear reactions	Unclassified—Unlimited Subject Category 93

19. Security Classif. (of this report)	20. Security Classif. (of this page)	21. No. of Pages	22. Price
Unclassified	Unclassified	12	A03

NASA FORM 1626 OCT 86

NASA-Langley, 1990

For sale by the National Technical Information Service, Springfield, Virginia 22161-2171